AGU PUBLICATIONS

Geophysical Research Letters

RESEARCH LETTER
10.1002/2016GL069330

Key Points:
- Humid air masses trigger Arctic sea ice melt by means of longwave radiation
- Melt preconditioning of the sea ice surface prior to melt onset
- Trends toward earlier melt onset linked to positive trends of longwave radiation in spring

Supporting Information:
- Supporting Information S1

Correspondence to:
G. Svensson,
gunilla@misu.su.se

Citation:
Mortin, J., G. Svensson, R. G. Graversen, M.-L. Kapsch, J. C. Stroeve, and L. N. Boisvert (2016), Melt onset over Arctic sea ice controlled by atmospheric moisture transport, *Geophys. Res. Lett.*, *43*, 6636–6642, doi:10.1002/2016GL069330.

Received 25 APR 2016
Accepted 1 JUN 2016
Accepted article online 3 JUN 2016
Published online 28 JUN 2016

Melt onset over Arctic sea ice controlled by atmospheric moisture transport

Jonas Mortin[1], Gunilla Svensson[1], Rune G. Graversen[2], Marie-Luise Kapsch[3], Julienne C. Stroeve[4,5], and Linette N. Boisvert[6]

[1]Department of Meteorology and Bolin Centre for Climate Research, Stockholm University, Stockholm, Sweden, [2]Department of Physics and Technology, UiT Arctic University of Norway, Tromsø, Norway, [3]Max-Planck-Institute for Meteorology, Hamburg, Germany, [4]National Snow and Ice Data Center, Cooperative Institute for Research in Environmental Sciences, University of Colorado Boulder, Boulder, Colorado, USA, [5]Centre for Polar Observation and Modelling, Earth Sciences/Department of Space and Climate Physics (MSSL), University College London, London, UK, [6]Earth System Science Interdisciplinary Center, University of Maryland, College Park, Maryland, USA

Abstract The timing of melt onset affects the surface energy uptake throughout the melt season. Yet the processes triggering melt and causing its large interannual variability are not well understood. Here we show that melt onset over Arctic sea ice is initiated by positive anomalies of water vapor, clouds, and air temperatures that increase the downwelling longwave radiation (LWD) to the surface. The earlier melt onset occurs; the stronger are these anomalies. Downwelling shortwave radiation (SWD) is smaller than usual at melt onset, indicating that melt is not triggered by SWD. When melt occurs early, an anomalously opaque atmosphere with positive LWD anomalies preconditions the surface for weeks preceding melt. In contrast, when melt begins late, clearer than usual conditions are evident prior to melt. Hence, atmospheric processes are imperative for melt onset. It is also found that spring LWD increased during recent decades, consistent with trends toward an earlier melt onset.

1. Introduction

The seasonal transition from winter to summer plays an important role for the Arctic climate. The timing of sea ice melt onset affects the energy absorbed by the surface throughout the summer melt season, because after melt begins, the albedo continues to decrease until either the sea ice is completely melted and disappears or freeze-up has begun [*Perovich and Polashenski*, 2012]. Over multiyear ice, for any day melt begins earlier, and additional energy sufficient to melt 3 cm of sea ice during the melt season is absorbed [*Perovich et al.*, 2007]. Since melt onset has been occurring successively earlier over the last few decades, the energy uptake over the Arctic Ocean in summer has increased by an amount large enough to melt about 1 m of ice over a recent 5 year period [*Stroeve et al.*, 2014]. This additional energy warms the ocean during summer, leading to a substantially later fall freeze-up [*Stroeve et al.*, 2014] and a warmer lower atmosphere in the fall [*Kurtz et al.*, 2011; *Serreze et al.*, 2008; *Screen and Simmons*, 2010]. Hereby the atmospheric circulation, both within and outside of the Arctic region, may be altered [*Cohen et al.*, 2014]. Furthermore, the timing of the melt onset may have predictable skills regarding the following September sea ice minimum [*Kapsch et al.*, 2014; *Schröder et al.*, 2014].

Although the timing of melt onset is of large importance for the climate in the Arctic and beyond, the processes controlling the melt onset and its large interannual variability are understood only to a limited extent. The Arctic-wide melt onset varies by up to 3 weeks between years [*Mortin et al.*, 2014; *Stroeve et al.*, 2014], corresponding to at least 0.5 m of ice melt over the melt season [*Perovich et al.*, 2007], but locally and regionally, the interannual variability can be much larger [*Mortin et al.*, 2014; *Stroeve et al.*, 2014]. At a specific site and a certain year, the melt onset was found to be triggered by moist, warm air masses associated with synoptic-scale weather systems that augmented the atmospheric energy fluxes to the surface [*Persson*, 2012]. Part of the melt variability in the Arctic is explained by anomalies in downwelling longwave radiation at the surface (LWD) [*Maksimovich and Vihma*, 2012; *Barber and Thomas*, 1998], and studies based on a few years have shown that the Arctic melt onset is weakly linked to two atmospheric circulation indicators, the Arctic oscillation [*Belchansky et al.*, 2004] and the 500 hPa height [*Drobot and Anderson*, 2001]. However, no studies have succeeded in drawing general conclusions concerning the processes important for melt onset. So the question remains: what processes control the timing of melt onset and its large variability

and trends on an Arctic-wide scale and over long time periods? To approach this question, we analyze 35 years of ERA-Interim data [*Dee et al*., 2011] and independent melt onset data [*Markus et al*., 2009], in addition to 10 years of water vapor fields retrieved from the satellite-borne Atmospheric Infrared Sounder (AIRS) [*Chahine et al*., 2006].

2. Data and Methods

Melt onset dates are retrieved from the microwave radiometers Scanning Multichannel Microwave Radiometer, Special Sensor Microwave/Imager, and Special Sensor Microwave Imager and Sounder [*Markus et al*., 2009; *Stroeve et al*., 2014]. One advantage of using melt retrievals from microwave radiometers is that microwave emissions are directly related to the melt signature of ice and snow [*Markus et al*., 2009]. As ice and snow begin to melt, water forms on the surface and within the snowpack, altering the surface's dielectric properties and thereby its emissivity; the emissivity increases significantly as snow and ice become wetter. Therefore, melt initiation can be measured by the increase in liquid water. More specifically, the method of *Markus et al*. [2009] detects melt onset based on the temporal variability of brightness temperatures at 19 GHz and 37 GHz in different combinations, which are dominated by variations of the amount of liquid water at the surface [*Markus et al*., 2009]. The data set contains two occurrences of melt onset: early melt onset (EMO), representing the first time melt is detected, and continuous melt onset. We use the EMO parameter only—here referred to as melt onset—because we found this to be more closely connected to the atmospheric processes initiating melt. The melt data are utilized at a 25 km resolution for the period 1979–2013.

The atmospheric variables used in this study are from ERA-Interim reanalysis, provided by the European Centre for Medium Range Forecasts (ECMWF) [*Dee et al*., 2011]. ERA-Interim has been evaluated extensively for the Arctic region showing good performance for large-scale variables when compared with the limited available observations [*Jakobson et al*., 2012; *Lindsay et al*., 2014; *Serreze et al*., 2012; *Zygmuntowska et al*., 2012]. See Text S1 in the supporting information for a brief discussion on our confidence in different ERA-Interim fields in the context of this paper. The radiative fluxes and cloud water are 24 h forecasts initiated at 00 UTC; other fields are daily means of 6-hourly analyses. ERA-Interim data fields were obtained at a $0.75° \times 0.75°$ resolution for the period 1979–2013.

The total integrated column water vapor burden from AIRS and the Advanced Microwave Sounding Unit (AMSU-A) instruments on board the polar-orbiting Aqua platform [*Chahine et al*., 2006] are utilized to gain further confidence in the results and as an alternative to ERA-Interim (see Text S1). We employ level 3 (version 6) daily data provided at a spatial resolution of $1° \times 1°$ for the period 2003–2013 [*Susskind et al*., 2014]. This is considered a mature product [e.g., *Devasthale et al*., 2013].

ERA-Interim data are interpolated to a $1.5° \times 6°$ latitude-longitude grid, and AIRS data are interpolated to a $1° \times 4°$ grid. At 75°N, the interpolated ERA-Interim grid cells cover about 170 km, both meridionally and zonally. We have checked that the analysis is insensitive to these resolutions, as long as the resolution is equal to or higher than 3° by 12°. To analyze atmospheric data only for locations where melt occurs and to ensure data consistency between surface and atmospheric variables, we include only grid cells with at least five detected melt onset dates (obtained from the 25×25 km EMO data) during at least 5 years. Further, we exclude grid cells that contain more than 50% land. The anomaly analysis in Figure 1 is insensitive to these thresholds. The analysis includes 579 grid cells in total ($1.5° \times 6°$), spanning 46.5°N to 87.75°N (Figure 1a). The anomalies of ERA-Interim and AIRS data are computed as deviations from the daily climatologies of the full time periods, which are different for ERA-Interim (1979–2013) and AIRS (2003–2013). Time series of atmospheric anomalies relative to the melt dates are obtained and aggregated over each grid cell using an area-weighted mean. The Arctic sea ice domain is then divided into 13 regions [*Stroeve et al*., 2014] (Figure S1), and for each of these regions, five melt-timing quintiles (20th percentiles) are computed and used for a categorization of the melt dates (Figure 1b). The lowest quintile of the melt dates represents an anomalous early melt onset, while the highest quintile an anomalous late melt onset. The results are insensitive to the exact distribution and size of these regions. This division into regions is applied in order to take into account the large spatiotemporal variability and the meridional gradient of melt onset [*Markus et al*., 2009; *Mortin et al*., 2014]. Using the 13 regions is a trade-off between two extreme cases: using quintiles of the full sea ice cover would bias the late melt and early melt categories toward northerly and southerly located grid cells, respectively, while using quintiles of each grid cell would assume that all

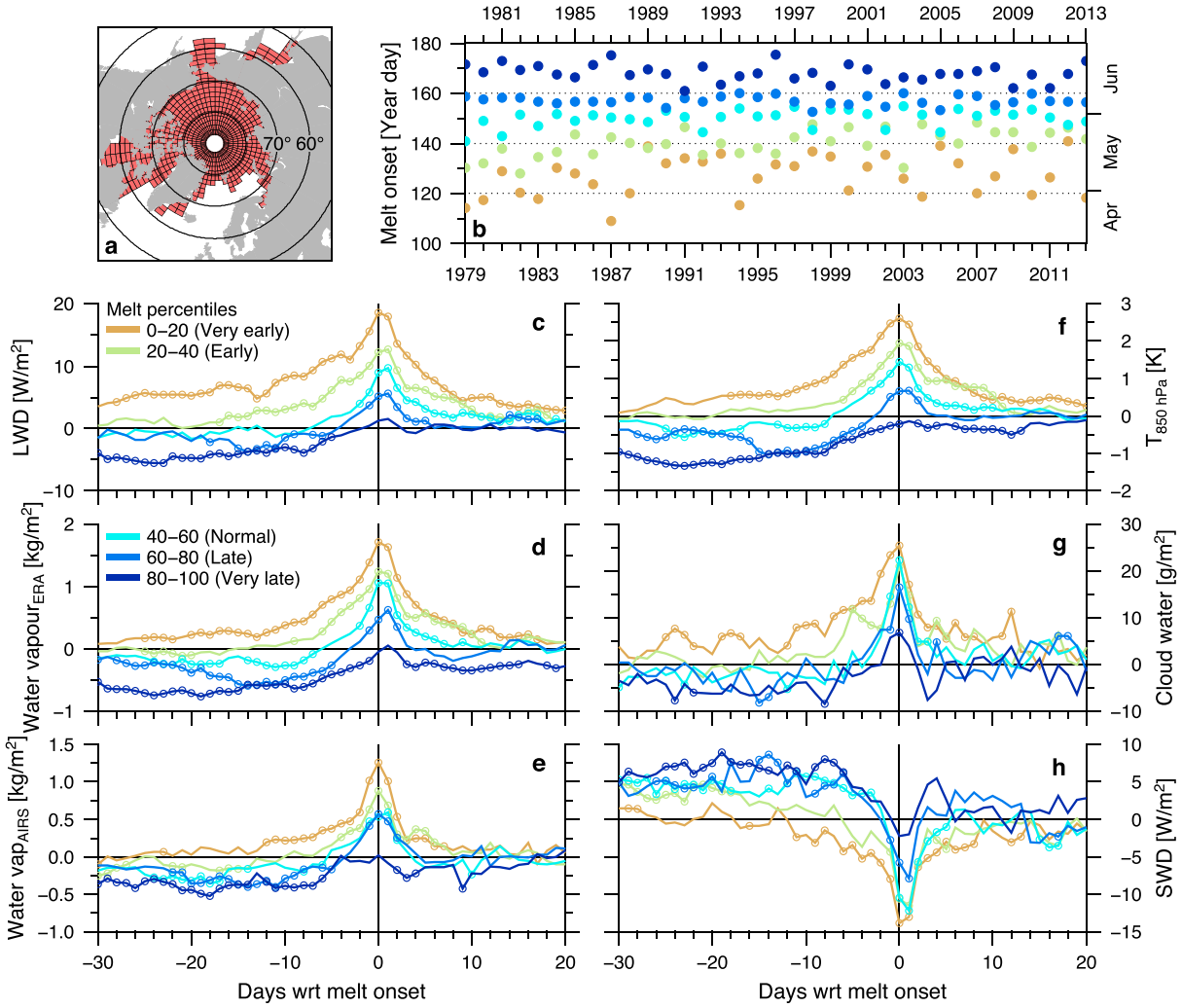

Figure 1. Study region, annual mean melt onset dates, and anomalies of atmospheric fields relative to the local melt onset date, presented as composites of the five melt onset categories introduced in section 2. (a) The grid and the study region. (b) Annual mean melt dates for each of the five categories of melt data (see Figures 1c and 1d for legend). Anomalies of atmospheric parameters from ERA-Interim (except in Figure 1e) for each melt category as a function of time lag relative to the local melt onset for (c) surface downwelling longwave radiation, (d) total column water vapor, (e) total integrated column water vapor burden retrieved from satellite (AIRS), (f) temperature at the 850 hPa pressure surface, (g) total column cloud water (liquid + ice), and (h) surface downwelling shortwave radiation. Dots in Figures 1c–1h indicate statistical significance ($p \leq 0.01$). For completeness, Figure S1 shows additional parameters.

categories of melt timing are represented in each grid cell, which may not be the case. Note that the date of melt onset for an early melt category can be later than the date for the subsequent category with a later melt date and vice versa (Figure 1b). This is a result of the large spatiotemporal variability of melt. The five categories are based on melt dates for the entire time period defined for each region individually. Averaging the values for each category and year over the 13 regions can result in a temporal variability of the mean dates of the different melt categories, primarily as melt onset dates are not normally distributed.

Statistical significance is determined using a two-tailed Student's *t* test on the aggregated time series for the null hypothesis that the distribution mean is equal to zero (Figures 1 and S1). Daily trends, discussed in section 5, are computed with an area-weighted least squares regression using all anomaly data of ERA-Interim (1979–2013) for a given year day.

3. Atmospheric State Around Melt Onset

Persson [2012] found that increased downwelling longwave radiation, due to advection of moist and warm air masses, triggered sea ice melt onset during one specific year and over a particular site. Here we use a similar

approach but instead analyze atmospheric parameters around the time of the melt onset on a pan-Arctic-wide area and long-term time scale. The Arctic melt onset dates are divided into five categories based on melt timing, from very early to very late melt (Figures 1 and S1). At melt onset, LWD at the surface exhibits significant positive anomalies, as a result of atmospheric water vapor, cloud water, and atmospheric temperature being larger than the long-term mean (Figures 1c–1g). This pattern is clear for all melt categories, for both ERA-Interim and AIRS, and positive anomalies are evident in a deep atmospheric column (Figure S2). AIRS exhibits weaker anomalies than ERA-Interim, most likely because of the shorter and later data period that constitutes the AIRS climatology (Figures 1d and 1e). The exception to the anomaly pattern is for the very late melt category, which instead exhibits negative anomalies prior to melt onset and normal conditions when melt begins (Figure 1). The increased cloudiness leads to a reduction of downwelling shortwave radiation at the surface (SWD; Figures 1g, 1h, and S2). These findings imply that the enhanced greenhouse effect associated with more moisture and clouds in the atmosphere is crucial for the timing of the melt onset over sea ice. Further, SWD in itself seems of minor importance for triggering melt. After melt is initiated, however, the importance of the SWD increases as the albedo of the sea ice surface decreases and more solar radiation is absorbed by the surface. Over sea ice, the albedo typically decreases from approximately 0.8 to about 0.5 after melt onset over sea ice [e.g., *Persson*, 2012; *Karlsson and Svensson*, 2013]. The atmospheric water vapor associated with the moisture and cloud anomalies is provided by atmospheric transport from remote areas rather than by local sources because the moisture and heat fluxes from the surface to the atmosphere are small over the sea ice covered ocean, especially prior to a large-scale melt event [*Boisvert et al*., 2013; *Persson*, 2012]. In addition, the moisture-transport convergence increases before and at melt onset (Figure S1). Hence, surface melt is triggered by increased LWD from transport of moisture into the Arctic.

The earlier the melt onset occurs, the stronger the atmospheric anomalies are (Figures 1, S1, and S2). Moreover, preconditioning of the surface is important for an early melt onset. For a very early melt onset (earliest 20%) LWD, water vapor, cloud water, and the atmospheric temperature all show significantly positive anomalies during a whole month preceding melt (Figures 1c, 1d, 1f, and 1g). During this month, positive anomalies are most likely a result of several smaller atmospheric events that individually are of insufficient strength to initiate melt, but their integrated enhanced greenhouse effect acts to raise the temperature of the snow-ice surface and the near-surface air temperatures, thereby preconditioning the surface for melt (Figure S1). This is consistent with in situ observations [*Persson*, 2012]. Again, once melt is initiated, the albedo decreases, resulting in the shortwave radiation becoming a strong amplifying factor to surface warming and melting of the snow-ice surface [*Persson*, 2012]. This effect seems particularly important for the early melt category, as indicated by positive anomalies of net shortwave radiation after melt onset (Figure S1c).

On the other hand, anomalously clear-sky conditions and negative anomalies of water vapor during spring lead coincide with a late melt onset (Figure 1). For the very late melt onset (latest 20%), atmospheric conditions during the month prior to melt are characterized by negative anomalies of water vapor and cloud water and colder-than-usual atmospheric and surface conditions (Figures 1d–1g, S1, and S2). Negative anomalies of water vapor and clouds reduce the greenhouse effect and lead to radiative cooling of the surface and delay the melt onset. The anomalously clear atmosphere also results in positive SWD anomalies during the month prior to melt onset (Figure 1h), yet the extra energy provided by SWD is insufficient to initiate surface melt since a large fraction of the SWD is reflected by the still snow-covered sea ice.

4. Spatial Variability of Atmospheric Anomalies and Surface Melt

The spatiotemporal variability of melt onset is consistent with the spatiotemporal variability of atmospheric moisture anomalies (Figure 2). These moisture anomalies exhibit a strong spatial variability (Figures 2a–2c are typical), are present in a deep atmospheric column (Figure S2), and are often a result of an interplay between midlatitude cyclones and atmospheric blockings [e.g., *Doyle et al*., 2011; *Woods et al*., 2013]. Retarded by the blockings, these cyclones either deflect poleward with their associated moisture or remain at midlatitudes, while creating sustained, narrow injections of moisture into the Arctic [*Woods et al*., 2013]. The narrow moisture structures may trigger melt over small areas, while the cyclones traversing the Arctic can trigger a spatially more extensive melt with their associated frontal systems and deep-layer moisture transport [*Persson*, 2012; *Stramler et al*., 2011]. Clouds associated with these humid air masses are important since they generate particularly strong positive anomalies of LWD [*Doyle et al*., 2011; *Persson*, 2012], especially clouds

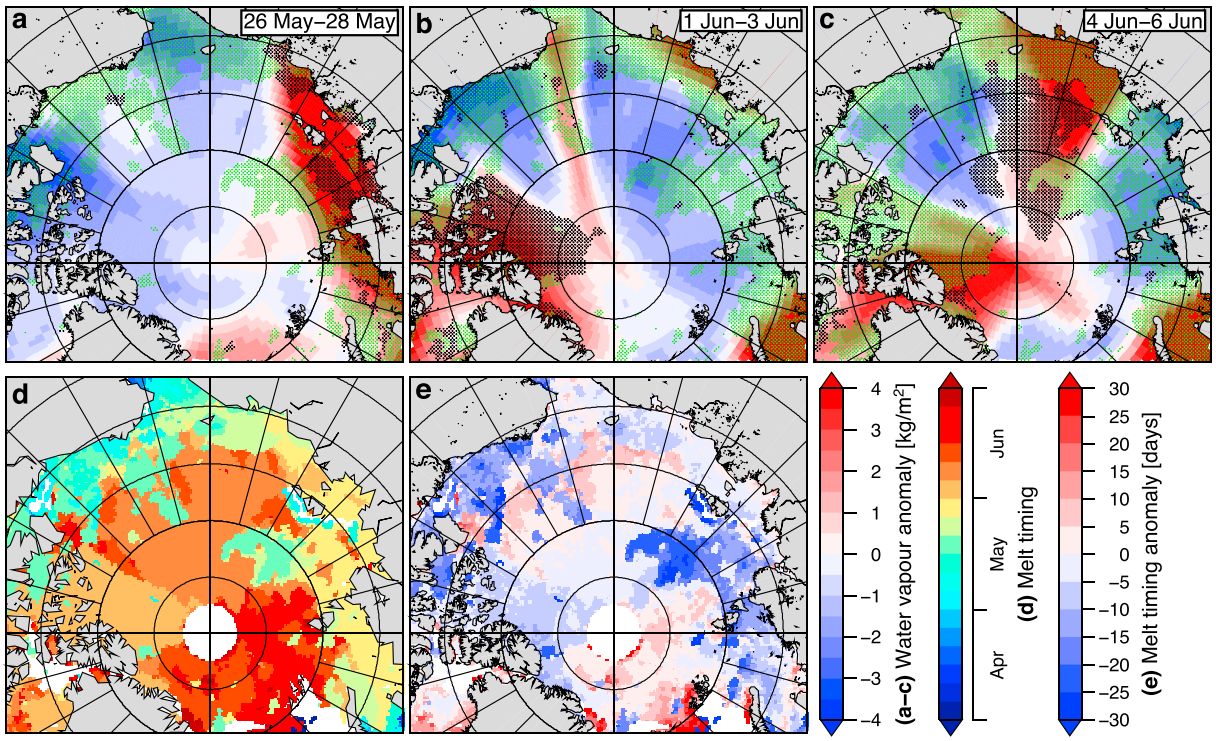

Figure 2. Example of melt onset and water vapor anomalies. (a–c) Snapshots of 3 day mean total column water vapor anomalies with the melt timing superimposed in the year 1991. Black dots mark areas where melt begins within the 3 day period, and green dots mark earlier initiated melt. (d) Melt timing. (e) Melt-timing anomalies (relative to the local climatology). Figure S3 shows all frames for 17 May through 12 June 1991.

containing liquid water [*Shupe and Intrieri*, 2004]. If the LWD anomalies from the cloudy and humid air masses are of insufficient strength to trigger melt for the given surface conditions in spring, they nevertheless act to increase the surface temperature [*Persson*, 2012], thereby preconditioning the surface for melt. Typically, the melt onset timing is similar over areas of at least 300–600 km (Figure 2d). Between these areas, strong gradients of melt timing are evident—commonly 3 week differences over short distances (Figure 2d)—mainly as a result of the strong spatial variability and transient behavior of the moisture and cloud water anomalies. The size of the areas of similar melt onset differs between years, following the spatial scale of the moisture anomalies (not shown). Note that the thickness distribution of snow, and to some extent sea ice, contributes to the large spatial variability of melt onset, due to the insulating properties of snow —the melting temperature at the surface is reached earlier for a thin snow layer than for a thick layer under similar atmospheric conditions.

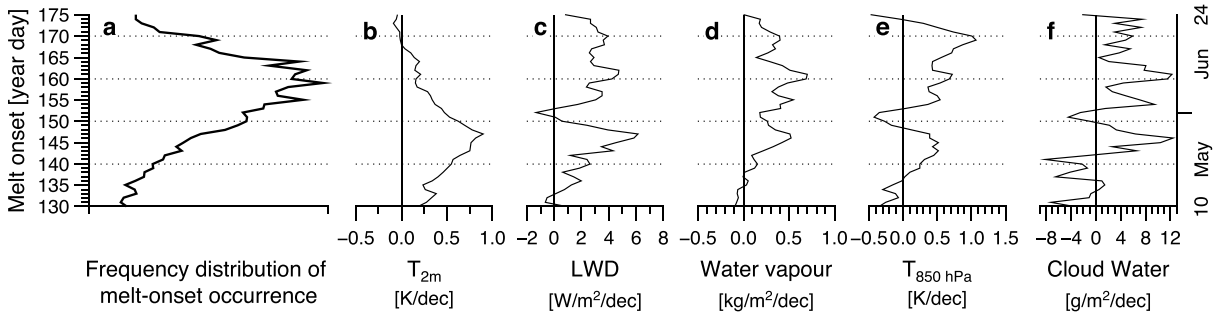

Figure 3. Histogram of melt onset timing and trends of pan-Arctic atmospheric parameters as a function of the day of the year. (a) Histogram of the pan-Arctic melt onset timing during 1979–2013. (b–f) Trends of (b), 2 m temperature, (c) downwelling longwave radiation at the surface, (d) total column water vapor, (e) atmospheric temperature at the 850 hPa pressure surface, (f) total column cloud water (liquid + ice) given in unit per decade. Annotations on right axis mark the day of the year. See section 2 for details on how the trends are computed.

5. Trends in Atmospheric Fields

Moisture anomalies increasing in intensity or frequency, or a combination of the two, during early spring would trigger an earlier melt onset. Positive pan-Arctic trends of LWD (about 6 W m^{-2}/decade) and near-surface temperature (about 0.8 K/decade) are found in spring, especially in late May (around day of the year 145; Figure 3a). These positive trends early in the season coincide with the observed tendency toward an earlier melt onset during recent decades [*Stroeve et al*., 2014]. The trends of the melt onset are mostly negative, indicating that early melt onset tends to occur earlier—early melt onset begins more than 2 days/decade earlier considering the whole Arctic (Table S1). Locally, early melt onset trends are larger and can reach up to 8 days/decade, e.g., in the Barents, East Greenland, and Kara Seas, as well as in the Baffin and Hudson Bay. The LWD trend is a result of increasing water vapor, air temperature—and to some extent—cloud water (Figures 3d–3f). This is consistent with previous findings of increasing trends of low-level clouds, moisture, atmospheric temperature, and thus LWD and near-surface temperature during recent decades [*Eastman and Warren*, 2010; *Francis and Hunter*, 2007; *Serreze et al*., 2012; *Boisvert and Stroeve*, 2015].

6. Conclusions

In conclusion, both for a late and an early melt onset, transport of humid, warm air over the Arctic sea ice area and the associated augmentation of the greenhouse effect appear to be the dominating processes for the initiation of surface melt. For an early melt onset, significant positive anomalies of total column water vapor, atmospheric temperature, and cloud water act in concert to induce the melt through enhanced LWD, whereas for late melt onset, it is rather a change from negative anomalies of these parameters to normal conditions that triggers the melt onset. These findings are in line with previous studies, showing that LWD explains a large fraction of melt onset variability in the Arctic [*Maksimovich and Vihma*, 2012; *Persson*, 2012]. We further discuss mechanisms that explain variations in LWD, and hereby the timing of melt onset. Our results suggest that in order to model the Arctic climate system properly, the representation of the atmospheric variability in spring, before and at melt onset, is the key. Finally, in light of continued warming of the Arctic region, we expect melt onset to continue to occur earlier in spring due to positive trends in LWD in the weeks prior to the present day melt onset. This shift toward an earlier melt has consequences for the climate of the Arctic and beyond.

Acknowledgments
The authors would like to thank Michael Tjernström for fruitful discussions on this subject. We further would like to thank the, in section 2, mentioned data centers and individuals collecting, computing, and supplying accessible high-quality data. ERA-Interim reanalysis are available from the ECMWF website (ecmwf.int) and AIRS and AMSU-A satellite retrievals from the Jet Propulsion Laboratory website (airs.jpl.nasa.gov). Melt data were obtained from the NASA Cryosphere Science Research Portal (neptune.gsfc.nasa.gov) and from Jeffrey Miller at NASA Goddard Space Flight Center.

References

Barber, D. G., and A. Thomas (1998), The influence of cloud cover on the radiation budget, physical properties and microwave scattering coefficient of first-year and multi-year sea ice, *IEEE Trans. Geosci. Remote Sens.*, *361*, 38–50, doi:10.1109/36.655316.

Belchansky, G. I., D. C. Douglas, and N. G. Platonov (2004), Duration of the Arctic sea ice melt season: Regional and interannual variability, 1979–2001, *J. Clim.*, *17*(1), 67–80, doi:10.1175/1520-0442(2004)017<0067:DOTASI>2.0.CO;2.

Boisvert, L. N., and J. C. Stroeve (2015), The Arctic is becoming warmer and wetter as revealed by the atmospheric infrared sounder, *Geophys. Res. Lett.*, *42*, 4439–4446, doi:10.1002/2015GL063775.

Boisvert, L. N., T. Markus, and T. Vihma (2013), Moisture flux changes and trends for the entire Arctic in 2003–2011 derived from EOS Aqua data, *J. Geophys. Res. Oceans*, *118*, 5829–5843, doi:10.1002/jgrc.20414.

Chahine, M. T., et al. (2006), AIRS: Improving weather forecasting and providing new data on greenhouse gases, *Bull. Am. Meteorol. Soc.*, *87*(7), 911–926, doi:10.1175/BAMS-87-7-911.

Cohen, J., et al. (2014), Recent Arctic amplification and extreme mid-latitude weather, *Nat. Geosci.*, *7*(9), 627–637, doi:10.1038/ngeo2234.

Dee, D. P., et al. (2011), The ERA-Interim reanalysis: Configuration and performance of the data assimilation system, *Q. J. R. Meteorol. Soc.*, *137*(656), 553–597, doi:10.1002/qj.828.

Devasthale, A., J. Sedlar, T. Koenigk, and E. J. Fetzer (2013), The thermodynamic state of the Arctic atmosphere observed by AIRS: Comparisons during the record minimum sea ice extents of 2007 and 2012, *Atmos. Chem. Phys.*, *13*(15), 7441–7450, doi:10.5194/acp-13-7441-2013.

Doyle, J. G., G. Lesins, C. P. Thackray, C. Perro, G. J. Nott, T. J. Duck, R. Damoah, and J. R. Drummond (2011), Water vapor intrusions into the high Arctic during winter, *Geophys. Res. Lett.*, *38*, L12806, doi:10.1029/2011GL047493.

Drobot, S. D., and M. R. Anderson (2001), Comparison of interannual snowmelt-onset dates with atmospheric conditions, *Ann. Glaciol.*, *33*(1), 79–84, doi:10.3189/172756401781818851.

Eastman, R., and S. G. Warren (2010), Interannual variations of Arctic cloud types in relation to sea ice, *J. Clim.*, *23*(15), 4216–4232, doi:10.1175/2010JCLI3492.1.

Francis, J. A., and E. Hunter (2007), Changes in the fabric of the Arctic's greenhouse blanket, *Environ. Res. Lett.*, *2*(4), 045011, doi:10.1088/1748-9326/2/4/045011.

Jakobson, E., T. Vihma, T. Palo, L. Jakobson, H. Keernik, and J. Jaagus (2012), Validation of atmospheric reanalyses over the central Arctic Ocean, *Geophys. Res. Lett.*, *39*, L10802, doi:10.1029/2012GL051591.

Kapsch, M.-L., R. G. Graversen, T. Economou, and M. Tjernström (2014), The importance of spring atmospheric conditions for predictions of the Arctic summer sea ice extent, *Geophys. Res. Lett.*, *41*, 5288–5296, doi:10.1002/2014GL060826.

Karlsson, J., and G. Svensson (2013), Consequences of poor representation of Arctic sea ice albedo and cloud-radiation interactions in the CMIP5 model ensemble, *Geophys. Res. Lett.*, *41*, 4374–4379, doi:10.1002/grl.50768.

Kurtz, N. T., T. Markus, S. L. Farrell, D. L. Worthen, and L. N. Boisvert (2011), Observations of recent Arctic sea ice volume loss and its impact on ocean-atmosphere energy exchange and ice production, *J. Geophys. Res.*, *116*, C04015, doi:10.1029/2010JC006235.

Lindsay, R., M. Wensnahan, A. Schweiger, and J. Zhang (2014), Evaluation of seven different atmospheric reanalysis products in the Arctic, *J. Clim.*, *27*(7), 2588–2606, doi:10.1175/JCLI-D-13-00014.1.

Maksimovich, E., and T. Vihma (2012), The effect of surface heat fluxes on interannual variability in the spring onset of snow melt in the central Arctic Ocean, *J. Geophys. Res.*, *117*, C07012, doi:10.1029/2011JC007220.

Markus, T., J. C. Stroeve, and J. Miller (2009), Recent changes in Arctic sea ice melt onset, freezeup, and melt season length, *J. Geophys. Res.*, *114*, C12024, doi:10.1029/2009JC005436.

Mortin, J., S. E. L. Howell, L. Wang, C. Derksen, G. Svensson, R. G. Graversen, and T. M. Schrøder (2014), Extending the QuikSCAT record of seasonal melt-freeze transitions over Arctic sea ice using ASCAT, *Remote Sens. Environ.*, *141*, 214–230, doi:10.1016/j.rse.2013.11.004.

Perovich, D. K., and C. Polashenski (2012), Albedo evolution of seasonal Arctic sea ice, *Geophys. Res. Lett.*, *39*, L08501, doi:10.1029/2012GL051432.

Perovich, D. K., S. V. Nghiem, T. Markus, and A. Schweiger (2007), Seasonal evolution and interannual variability of the local solar energy absorbed by the Arctic sea ice-ocean system, *J. Geophys. Res.*, *112*, C03005, doi:10.1029/2006JC003558.

Persson, P. O. G. (2012), Onset and end of the summer melt season over sea ice: Thermal structure and surface energy perspective from SHEBA, *Clim. Dyn.*, *39*(6), 1349–1371, doi:10.1007/s00382-011-1196-9.

Schröder, D., D. L. Feltham, D. Flocco, and M. Tsamados (2014), September Arctic sea-ice minimum predicted by spring melt-pond fraction, *Nat. Clim. Change*, *4*(5), 353–357, doi:10.1038/nclimate2203.

Screen, J. A., and I. Simmonds (2010), The central role of diminishing sea ice in recent Arctic temperature amplification, *Nature*, *464*(7293), 1334–1337, doi:10.1038/nature09051.

Serreze, M. C., A. P. Barrett, J. C. Stroeve, D. N. Kindig, and M. M. Holland (2008), The emergence of surface-based Arctic amplification, *Cryosphere*, *3*, 11–19, doi:10.5194/tc-3-11-2009.

Serreze, M. C., A. P. Barrett, and J. Stroeve (2012), Recent changes in tropospheric water vapor over the Arctic as assessed from radiosondes and atmospheric reanalyses, *J. Geophys. Res.*, *117*, D10104, doi:10.1029/2011JD017421.

Shupe, M. D., and J. M. Intrieri (2004), Cloud radiative forcing of the Arctic surface: The influence of cloud properties, surface albedo, and solar zenith angle, *J. Clim.*, *17*(3), 616–628, doi:10.1175/1520-0442(2004)017<0616:CRFOTA>2.0.CO;2.

Stramler, K., A. D. Del Genio, and W. B. Rossow (2011), Synoptically driven Arctic winter states, *J. Clim.*, *24*(6), 1747–1762, doi:10.1175/2010JCLI3817.1.

Stroeve, J. C., T. Markus, L. Boisvert, J. Miller, and A. Barrett (2014), Changes in Arctic melt season and implications for sea ice loss, *Geophys. Res. Lett.*, *41*, 1216–1225, doi:10.1002/2013GL058951.

Susskind, J., J. M. Blaisdell, and L. Iredell (2014), Improved methodology for surface and atmospheric soundings, error estimates, and quality control procedures: The atmospheric infrared sounder science team version-6 retrieval algorithm, *J. Appl. Remote Sens.*, *8*(1), 084994, doi:10.1117/1.JRS.8.084994.

Woods, C., R. Caballero, and G. Svensson (2013), Large-scale circulation associated with moisture intrusions into the Arctic during winter, *Geophys. Res. Lett.*, *40*, 4717–4721, doi:10.1002/grl.50912.

Zygmuntowska, M., T. Mauritsen, J. Quaas, and L. Kaleschke (2012), Arctic clouds and surface radiation—A critical comparison of satellite retrievals and the ERA-Interim reanalysis, *Atmos. Chem. Phys.*, *12*(14), 6667–6677, doi:10.5194/acp-12-6667-2012.